Available online at www.sciencedirect.com
ScienceDirect
International Journal of Solids and Structures 44 (2007) 1880–1890
INTERNATIONAL JOURNAL OF SOLIDS and STRUCTURES
www.elsevier.com/locate/ijsolstr

On dissolution driven crack growth

Per Ståhle [a], Christina Bjerkén [b,*], Andrey P. Jivkov [c]

[a] *Div. Solid Mechanics, Lund University, SE-21100 Lund, Sweden*
[b] *Div. Materials Science, Malmö University, SE-20506 Malmö, Sweden*
[c] *School of Materials, The University of Manchester, Manchester M601QD, UK*

Received 2 May 2006; received in revised form 11 September 2006
Available online 19 September 2006

Abstract

The formation and growth of a crack in a body subjected to stress driven material dissolution is studied. The rate of material dissolution is proportional to strain energy and curvature of the body surface. The formation of a crack from a plane surface is preceded by an evolving surface roughness. The continued dissolution enhances roughness amplitude resulting in pit formation. As the pit grows deeper into the material, it assumes the shape of a crack. The sharpness of the crack reaches its maximum during this transition from a pit to a crack. As the crack grows, a self-similar state is gradually assumed. During this phase characteristic lengths of the crack shape scale with the crack length. In line with this the crack progressively becomes blunt. The widest part of the crack when unloaded is in the vicinity of the crack tip. A consequence of the model is that no criterion is needed for crack growth. Neither is a criterion needed for determination of the crack path. It also follows that the crack growth rate is almost independent of the remote load. Further, spontaneous crack branching is anticipated. A motivation for this is given.

Keywords: Stress corrosion; Crack growth; Crack initiation; Branching

1. Introduction

During stress corrosion, loss of dissolved metal ions leads to pitting and formation of cracks. This is followed by growth of one or several of the cracks. The dissolution process starts if bare metal is exposed to aggressive environments. This can be a bulk aqueous environment surrounding the body or micro environment, such as in pits, crevices or under deposits, or even created by microbes that are active on the surface. Often, an impermeable film of mainly metal oxides and hydroxides are formed by dissolved metal. Even though the thickness of this film is typically not more than 1–4 nm, it reduces the rate of dissolution by several orders of magnitude, cf. [(MacDonald, 1999)]. An adherent protective film increases the life of structural members tremendously. However, the film may be damaged, e.g., as a result of cyclic loading, variations in

* Corresponding author. Tel.: +46 40 6657626.
E-mail addresses: per.stahle@ts.mah.se (P. Ståhle), christina.bjerken@ts.mah.se (C. Bjerkén), andrey.jivkov@manchester.ac.uk (A.P. Jivkov).

0020-7683/$ - see front matter
doi:10.1016/j.ijsolstr.2006.09.011

the electro-chemical environment or, as is recently discovered, by microbiological activity where the substrate material is involved in the metabolism of the microbial species (cf. ASME, 2003; Beech and Sunner, 2004). Assuming that the protective film is either repeatedly damaged or is not able to heal, leads to a moving boundary problem. In earlier studies by Jivkov, cf. Jivkov (2004), the dissolution is assumed to be a function only of the stretching of the surface and a threshold strain is invoked to comply with the properties of the oxide film.

When a means of mass transportation such as dissolution or surface diffusion is present mechanical stress has been observed to produce a surface waviness, which was first reported by Grinfeld (1986). The phenomenon when mass is transported through surface diffusion is theoretically explained by Asaro and Tiller (1972) and Srolovitz (1989). Mass transportation through dissolution to a surrounding environment, such as an etchant, is considered by Kim et al. (1999). The spectrum of the waves depends on the stress in the body surface and the surface energy. In both cases the theory is based on the recognition of the surface energy and the elastic strain energy providing driving forces for material dissolution. A large surface energy diminishes the waviness and a large elastic strain energy increases the waviness. For long wavelengths the elastic strain energy dominates and for short wavelengths the surface energy. The result is that waves with wave lengths longer than a stress-dependent critical value grow, while waves with shorter wavelength decay with time. Experimental results by Kim et al. (1999) show that the typical spatial wavelength in aluminium is on the scale of a few hundred nanometres when the stress is large and compare to the yield stress.

A linearized theory assuming that the amplitude of the height variation of the body surface is small leads to symmetric growth in the sense that growth rate of peaks, as an average, is the same as the growth rate of troughs (cf. Kim et al., 1999; Asaro and Tiller, 1972). Non-linear solutions show that, as the amplitude increases, the troughs grow faster and the growth rate of peaks decay (Yang and Srolovitz, 1994; Chiu and Gao, 1993; Spencer and Meiron, 1994; Kohlert et al., 2002). It was also observed that the process become localized leading to corrosion pits. It was found that the pits seemingly approach a singular state where the sharpest parts of the troughs assume the local geometry of an ideally sharp crack tip.

In the present article, it is demonstrated how a pit becomes a crack. In a strict sense it is a deep notch with a relatively sharp tip. Fig. 1 shows a real stress corrosion crack in a nuclear pressure vessel. This real crack has many features in common with the present results. The crack tip always preserves a finite radius, and, as opposed to the previous investigators, the present authors believe that there is a minimum crack width that depends on the crack tip driving force. It is explained in Section 4 how the crack becomes very thin and why then the growth assumes a local steady state. In Section 5 the steady-state conditions are examined. These conditions are the key to why the pit does not develop a cusp. Instead growth continues and a blunted crack is formed. The implications for a solitary crack are discussed in Section 6. The solitary growing crack enters a self-similar state in the sense that the width increases with the crack length for a fixed remote load. In this section also probable crack branching is discussed even though convergence problems put an end to the calculations before that happened.

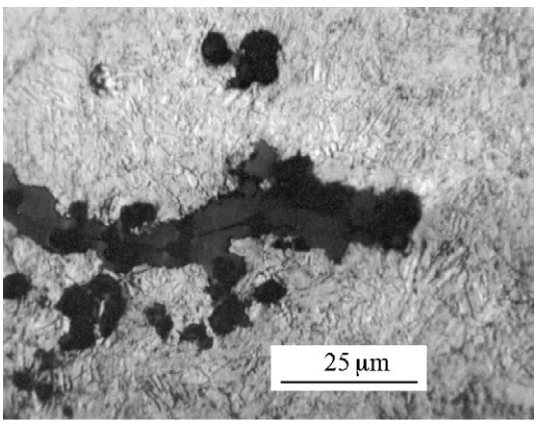

Fig. 1. Corrosion crack in a pressure vessel steel of type SA533C11. Note that the widest part of the crack is at the crack–tip. Crack length is 7 mm and notch width is around 10 μm. Reproduced with permission from Vattenfall AB, Sweden.

2. The model

In this paper two forms of energy that affect the rate of material dissolution are considered, i.e., elastic strain energy, w_e, and surface energy, w_s. The variations of these energies are assumed to be the only driving forces evolving the surface morphology. The material is assumed to be elastic with a modulus of elasticity E and Poisson's ratio v. A plane stress state is studied. The result for plane strain can be obtained by simply replacing E with $E/(1-v^2)$. Strains ϵ_{ij} are assumed to be small. Stresses σ_{ij} and strains are related through Hooke's law $\sigma_{ij} = (E/(1+v))\epsilon_{ij} + \delta_{ij}(vE/(1+v))\epsilon_{kk}$. Indices i, j and k assume the values 1 and 2. The elastic strain energy density is given by the stresses and the strains as follows:

$$w_e = \frac{1}{2}\epsilon_{ij}\sigma_{ij} = \frac{1}{2E}\sigma_{ij}\sigma_{ij}. \tag{1}$$

Einstein's summation convention applies. The surface energy density is given as follows:

$$w_s = g_0 + \gamma\kappa, \tag{2}$$

where g_0 is the surface energy density of a flat solid surface, γ is the interfacial energy per unit of area and κ is the curvature of the surface (Kim et al., 1999). The curvature is defined positive if the surface is convex, i.e. if the centre of the curvature is towards the interior of the body. Here the mass removal rate is manifested as advance of the body surface in the inward direction. The environment serves as an inexhaustible absorber or provider of metal ions. Fig. 2 sketches how material is removed from or deposited to the surface making the boundary between the body and the environment move to accommodate the volume change. The advance rate of the body surface is assumed to depend on the densities of strain energy and surface energy as follows:

$$v_i = M(w_s + w_e)n_i = M\left(\frac{1}{2E}\sigma_{kl}\sigma_{kl} + g_0 + \gamma\kappa\right)n_i, \tag{3}$$

where M is assumed to be a constant that depends only on the environment. The vector n_i is the inward normal of the body surface, see Fig. 2.

Consider a large body with a straight traction free edge. The body initially occupies the region $x_1 \geqslant 0$. At large distances a uniaxial stress, σ_0, is applied parallel with the edge, i.e. along the x_2-direction. Therefore, the boundary conditions are:

$$\sigma_{11} = 0, \quad \sigma_{22} = \sigma_0 \quad \text{and} \quad \sigma_{12} = 0, \tag{4}$$

and along the traction free edge, initially at $x_1 = 0$

$$\sigma_{11} = \sigma_{12} = 0. \tag{5}$$

As the boundary evolves during material dissolution, the edge no longer coincides with $x_1 = 0$. Assuming that the modified edge has the normal n_i, the boundary conditions (5) are replaced with the following:

$$\sigma_{i1}n_i = \sigma_{i2}n_i = 0, \tag{6}$$

along the edge. The stresses are assumed to be in a quasi-static equilibrium. Equilibrium and compatibility of strains may be represented by the equations

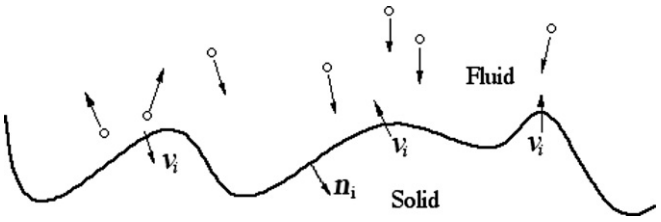

Fig. 2. Metal ions are immediately absorbed by the environment as they are detached from the body. Chemical conditions are assumed to be unaffected and the fluid plays the role of an inexhaustible buffer.

$$\sigma_{ij,j} = 0 \quad \text{and} \quad \sigma_{ii,jj} = 0. \tag{7}$$

In addition to this, material is removed from the edge, with a rate v_i given by (3). The evolving surface is assumed to remain traction free in agreement with (6). A non-dimensional form for (3) reads

$$\hat{v}_i = -\left(\hat{g}_0 + \frac{1}{2}\hat{\sigma}_{kl}\hat{\sigma}_{kl} + \hat{\kappa}\right)n_i, \tag{8}$$

where $\hat{v}_i = Ev_i/M\sigma_0^2$ and $\hat{g}_0 = Eg_0/\sigma_0^2$, $\hat{\sigma}_{kl} = \sigma_{kl}/\sigma_0$ and $\hat{\kappa} = E\gamma\kappa/\sigma_0^2$. Eqs. (4)–(7) are readily put in non-dimensional form after division by σ_0.

The constant $\hat{g}_0$ is assumed to be insignificant in the remaining part of the work. Initially when the waves forming on the surface are shallow the effect of $\hat{g}_0$ is a translation of the surface. During the evolution of pits and cracks the remaining terms of (8) are assumed to dominate due to relatively large stress and curvature that follows with the development of a pit or a crack.

A consequence of the scaling of (8) is that all the lengths scale with $E\gamma/\sigma_0^2$ and the time scales with $E^2\gamma/(M\sigma_0^4)$. Both length scale and time scale are relevant to the present study. A length parameter may be defined as

$$\lambda = \frac{4\pi E\gamma}{\sigma_0^2}, \tag{9}$$

and a time parameter is defined as

$$\tau = \frac{2\pi E^2\gamma}{M\sigma_0^4}. \tag{10}$$

The initial evolution of a virtually plane surface develops a roughness, where the dominating wave length equals λ. Wave lengths shorter than $\lambda/2$ do not develop but are instead attenuated (cf. e.g. Kim et al., 1999), where the plane strain result can be converted to the present plane stress result by replacing E with $E/(1-\nu^2)$.

3. Numerical analysis

A computational method that evolves a body surface by an adaptive finite element procedure is used, cf. (Jivkov, 2003, 2004). The method is based on a problem split into equilibrium and evolution sub-problems at each time increment. The equilibrium sub-problem, i.e. the solution of (4)–(7) is obtained using the finite element code ABAQUS (2004). Six-node triangular elements are used. The numerical procedure is based on the principle of virtual work. Virtual displacements δu_i and corresponding virtual strains, $\delta\epsilon_{ij}$ as variations of parameterized displacement functional, give the following equation for the first variation of the total potential energy

$$\delta U = \frac{1}{2}\int_V \delta\epsilon_{ij}\sigma_{ij}\mathrm{d}V - \int_S \delta u_i\sigma_{ij}n_j\,\mathrm{d}S. \tag{11}$$

The body volume V is bounded by the surface S. The solution is obtained as

$$\delta U/\delta u^{(\mathrm{n})} = 0, \tag{12}$$

where $u^{(\mathrm{n})}$ are nodal displacements.

At time t, the solution to (12) provides the distribution of stress along the surface. The stress in the body surface, along with curvature of the surface, gives the dissolution rate and the new position of the body surface as

$$h_i(t+\Delta t) = h_i(t) + \Delta t v_i(t), \tag{13}$$

where the $h_i(t)$ defines the position of the surface as a function of the time t, and v_i is given by (3) or in non-dimensional form by (8). This presents the evolution sub-problem, which is solved using an in-house procedure for surface tracking and geometry re-meshing. In the finite element environment, the surface advance

is represented by surface node displacements. To ensure that the incremental evolution of the surface is not accelerating due to developing stress concentrations eventually resulting in numerical problems, a maximum corrosion depth is governing size of the time step, Δt, in each computational step. This maximum penetration depth used in the present study is of the same order of magnitude as the side length of the smallest element.

A problem for moving boundaries was studied by Zhang and Bower (1999), using a finite element method, where a differential equation had to be solved to compute the advancing of the body boundaries. The mesh was updated in increments the same way as done in the present analysis. The character of the problem allowed them to preserve principle meshing throughout the calculations. The present problem creates an extensive amount of new surfaces. Because of that the mesh has to be totally rearranged during the calculations. Here this is done at every increment. To properly follow the surface shape changes, a new distribution of nodes along the evolved surface is essential. The existing nodes along the evolving surface at the beginning of a time step define the positions of the same number of points along the advanced surface at the end of the time step. A B-spline curve is created along the new surface using these node positions as spline knots (Knott, 1999). New nodes along that curve are distributed using a surface refinement process, based on one curvature and two length constraints. At every step of the surface refinement process, the nodes already introduced form a polygon of line segments. The curvature constraint is given by the maximum angle that two neighbouring segments are allowed to make. The length constraints specify the maximum and the minimum allowed node spacing. The maximum node spacing is used to initially distribute nodes along the B-spline at regular distances. After this initial meshing, the refinement procedure is based on segment splitting using the maximum angle and minimum distance constraints. A thorough description of the refinement process may be found in Jivkov (2003). The evolved body geometry requires re-meshing of the interior, which is completed with a Delaunay-type triangulation procedure (Shewchuk, 2002). Thus, the current geometry is changed and the finite element formulation of the boundary value problem for the next time increment is prepared. The ratio between element sides of the smallest element and the characteristic length scale of the problem is typically 0.005λ. A typical mesh is displayed in Fig. 3.

Overall, the solution is handled by the procedure for the evolution sub-problem. At each increment of time, this procedure prepares the mesh for the current boundary value problem, invokes ABAQUS as an external solver and waits for the equilibrium results to be delivered in order to decide for future surface evolution.

During the calculations the minimum length between nodes, $l_{\min}$, was varied as $\lambda/10$, $\lambda/20$, $\lambda/40$, $\lambda/80$, i.e. reducing the length parameter of the mesh by dividing with 2. Also the maximum length between nodes ($l_{\max} = 10 l_{\min}$) and the maximum distance of evolution governing the time increment ($l_{\text{adv}} = l_{\min}$) were reduced correspondingly. For the case with a coarse mesh ($l_{\min} = \lambda/10$), the deep pits were not formed and there was abnormal undulations of the surface. For finer mesh parameters, the wavy surface evolved into pits that deepened. The finer the mesh, the more a cusp-like shape was obtained, i.e. that means to say that the maximum curvature was obtained for the finest mesh investigated. For this mesh the computational efforts became too

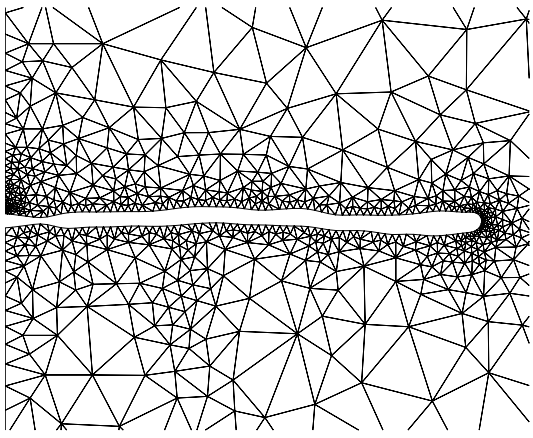

Fig. 3. Typical mesh for a crack starting from an surface indent.

large and the stage were the pit develops into a crack could not be investigated. The width of the cracks for the two intermediate cases showed that the width of the crack for finer mesh was approximately 0.7 of the coarse mesh. This indicates a somewhat slow convergens of present model. The largest differences is for a pit depth of around 0.2λ to 0.5λ. The convergence rate is better for shallow waves and for large cracks.

4. Pitting

To evaluate the model the evolution of a small amplitude randomly perturbed surface is computed. In the initial surface the nodes along the free edge are dislocated at $x_1 = 0$ and $-b < x_2 < b$, where the remote load is selected so that b becomes around 10λ. Every node in this section is given an initial position that is a random distance in the x_1-direction. The distances are rectangularly distributed in the interval -0.01λ to 0.01λ. A Fourier transform of the result shows that high frequency waves diminish and that a dominating peak in growth rate develops for wave lengths that approximately equals λ. The expected wave length of the fastest growing perturbations is λ (cf. Srolovitz, 1989).

To further study the behaviour of the model for different wavelengths, an initially sine-wave perturbed surface was used with a fixed wavelength λ_0 and the numerical value of the length scale λ was changed. The initial surface was given a maximum displacement of $0.05\lambda_0$. This perturbed surface covered around 10 periods of a cosine wave along the x_2-axis, i.e., $x_1 = \cos(2\pi x_2/\lambda_0)$. For λ larger than $2.0\lambda_0$ the amplitude is reduced during the simulation. This is expected, given that the critical wave length is $(1/2)\lambda$.

At least initially, the fastest growing waves was, as in the simulation of a randomly perturbed surface, obtained for $\lambda = \lambda_0$. Fig. 4 shows how the surface evolves for $\lambda = \lambda_0$. The last position of the pit in this figure is when the largest curvature of the tip is reached. This position defines the time $t/\tau = 0$. The time spent before this is ambiguous since the extent of the phase with shallow waves depend strongly on the amplitude selected for the initial waves.

Initially the amplification of the original waviness is observed to be linear, which, e.g., is manifested as a symmetric growth of convex and concave half periods. When the amplitude becomes of the order of, say a tenth of λ, the shape becomes clearly asymmetric. After that, more or less only the inward going parts of

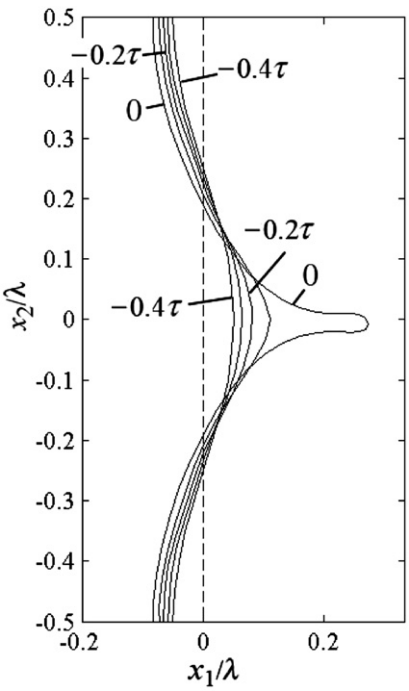

Fig. 4. Development of a pit. The wavelength of an initial sine-wave equals λ.

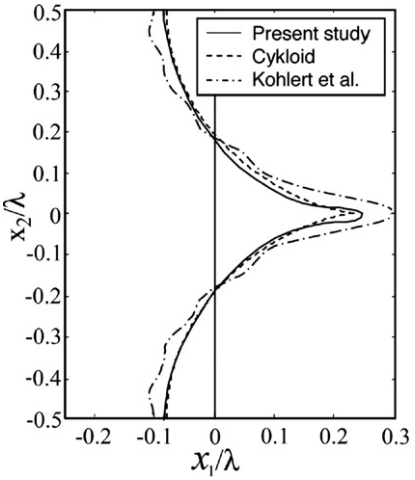

Fig. 5. Comparison of final pit shape obtained by Kohlert et al. (2002) and a cycloid compared with the present result.

the surface grow. At $t/\tau = 0$ a somewhat cusp-like shape is obtained. A curvature of around $50/\lambda$ is obtained at $t/\tau = 0$. This occurs when the depth of the pit is around 0.3λ as shown in Fig. 4.

It has been suggested that the surface after some time assumes the shape of a cycloid at least for diffusion driven cracks (cf. Kohlert et al., 2002; Chiu and Gao, 1993). The parametric form of the cycloid chosen here is

$$x_1 = \lambda(2\pi)(1/2 + \cos\xi) \quad \text{and} \quad x_2 = \lambda/(2\pi)(\xi - \sin\xi), \tag{14}$$

where x_1 and x_2 define the position of a cycloid surface. Fig. 5 compares the present result with the result of Kohlert et al. (2002). A cusp shape is also included in the figure. In the solution by Kohlert et al. (2002), short wave ripples are observed on the flanks surrounding the pit. This is supposed to indicate that the employed series expansion nearly fail to converge. Apart from these ripples all three results at a selected stage of the present solution, coincide fairly well. It is assumed by Kohlert et al. (2002) that a cusp solution is approached also for his model. A significant property of a cusp or a sharp crack is the width and shape of the crack tip. At a certain depth, the tip of the pit is supposed to degenerate to become a singular point. However, the present calculation does not result in a cusp. Instead, after the minimum tip radius is obtained, the tip widens during continued growth, as is described in the following section.

5. Initiation of cracks and self-similar crack growth

The pit may develop from a random surface roughness or from single frequency waves, as described in the previous section. It may also develop from a pre-existing indent that may have caused the dissolution to localize. With a periodic wavy surface an array of co-linear pits is formed. When the pits have grown beyond the time $t/\tau = 0$ they form cracks. The simulations indicate that the competition between the growing cracks makes the growth rate unstable. Therefore, only one or two of 10 co-linear pits simulated in the previous section continue to become substantially large cracks. The process is likely to continue until only one crack remains but this could not be done within reasonable computation time. Instead, here, a solitary crack is analysed.

Fig. 6 shows how a formed crack extends while the blunting of the tip increases. The time elapsed since the transformation from pit to a crack, defined as $t/\tau = 0$, to the present situation is $t = 1.5\tau$. The slightly sloping crack is the result of a not fully stable path. As the crack grows the crack tip driving force increases. The stress intensity factor, K_I, is depending on geometry, only via the length of the crack, a. In this situation, when the crack tip radius, is increasing, the strain energy is the only term in (3) that increases. The surface energy density decreases. Therefore, the strain energy increasingly dominates as a driving force for crack growth. This leave us with a dominating length scale, $(K_I/\sigma_0)^2$ or equivalently the crack length, a.

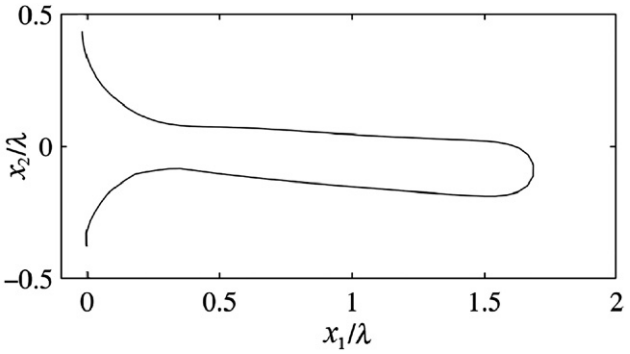

Fig. 6. The development of a crack initiated from a pit. The non-dimensional time elapsed is $t/\tau = 1.5$. The slightly sloping crack is the result of a not fully stable path.

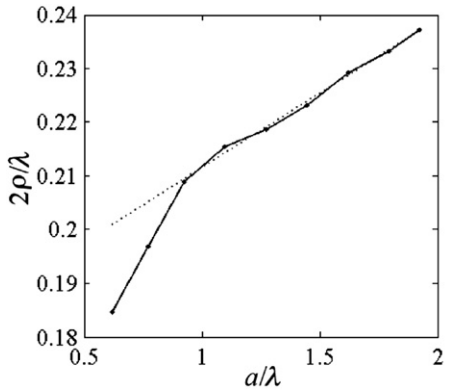

Fig. 7. Normalised width, $2\rho/\lambda$, versus normalised crack length, a/λ.

The width of the crack increases as is shown in Fig. 7. When the crack length $a \geqslant \lambda_0$ the width increases approximately linearly with crack length. At this stage the solution has assumed an approximate self-similar state, i.e. all characteristic lengths of the evolving geometry, scale with the crack length. The length scale originates from the growth rate, v_{tip}, at the deepest part of the pit and the time t through $a = \int v_{\text{tip}}\,\mathrm{d}t$. Fig. 7 give the following relation between crack width, 2ρ, and the crack length

$$2\rho = 0.027a. \tag{15}$$

A more general relation is obtained by using the stress intensity factor for an edge crack, i.e. $K_{\text{I}} = 1.12\sigma_0\sqrt{\pi a}$. The relation (15) gives

$$2\rho = 0.007(K_{\text{I}}/\sigma_0)^2. \tag{16}$$

Consider that the origin of the coordinate system x_1 and x_2 is at the crack mouth $r = \sqrt{x_1^2 + x_2^2}$. If the shape of the crack should remain constant the dissolution rate v_i projected on the vector x_i has to be constant at every point along the surface, as the lower part of Fig. 8 shows. At the crack tip the dissolution rate is v_{tip}. Therefore, self-similar growth requires that the dissolution rate at all points of the crack surface fulfil the self-similarity condition

$$v_i = v_{\text{tip}}\frac{n_j x_j}{r}n_i, \tag{17}$$

where r is the distance from the crack mouth and n_i is the inward unit normal of the surface.

The calculations show that the width is very small as compared with the crack length. The image of an idealized crack therefore seems appropriate and (17) may, by putting $x_2/x_1 = 0$, be replaced with the steady-state condition

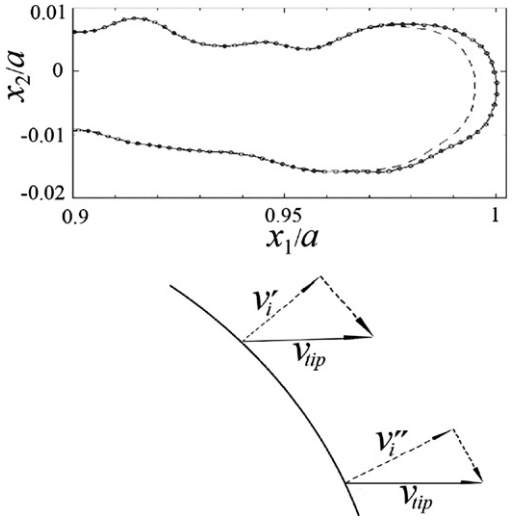

Fig. 8. The tip of the steady-state growing crack. Note that the crack surfaces are slightly swaying. The lower insert shows the requirement that the dissolution rates are constant in the x_1-direction at all points of the crack surface according to (18).

$$v_i = v_{\text{tip}} n_1^2 n_i. \tag{18}$$

In Fig. 8 the dashed curve shows the position of the crack at an earlier time increment. The result confirms that the dissolution rate is small on the crack surfaces whereas the major dissolution occurs at the tip.

Further, another consequence of the self-similar crack growth is that the stress distribution remain constant in the crack tip region. The stress at the crack tip, σ_{tip}, observed when the crack length a is larger than λ is around $23\sigma_0$. On the flanks of the blunted tip the stress rapidly decreases. At a horizontal distance of ρ from the crack tip the stress has decreased to around $4\sigma_0$.

6. Discussion

The simulations show that there is an initial phase when the pit sharpens and becomes a crack. At this point the shape is fairly well approximated by that of a cycloid. The deepest part of the cycloid is a cusp. Locally the surfaces of the cusp are parallel and the tip is a point. Therefore, the cusp tip neighbourhood is that of a crack and in the cusp tip neighbourhood a square root singular stress field dominates.

The stress intensity factor of the tip was calculated by Chiu and Gao (1993) to be

$$K_{\text{I}} = \sigma_0 \sqrt{\lambda/2}, \tag{19}$$

where the period length of the initial wavyness, i.e., the distance between the cusps, $\lambda_0 = \lambda$. The slightly sloping crack is the result of a not fully stable path. There is not any path criteria in the present calculations and because of that the path is slightly unstable. The slightly sloping crack is the result a numerically trigged deviation from a straight path (cf. Bjerkén et al., 2006). The width of a crack with the stress intensity factor given by (19) should according to (16) be related to λ as follows:

$$2\rho = 0.0035\lambda, \tag{20}$$

which is around 0.13 of the present result as observed in Fig. 4. It is the observation also from Fig. 7 that there is a rapid increase in crack tip radius when the crack is growing to the length λ. This could be an effect of the assumed steady-state conditions and it could also be an effect of the slow convergence of the model.

The results for self-similar crack growth provide insight into the possibly paradoxical result that the crack does not continue to sharpen as it grows. It is first noted that any sharp crack would be in a local state of self-similar growth. In view of the result, a crack that is sharper than given by (16) with respect to the remote stress intensity factor would suffer from large stresses along the approximately straight crack surfaces where the

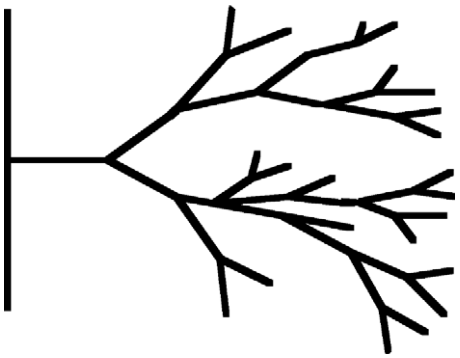

Fig. 9. Repeated branching leads to a crack geometry with preserved self-similar properties.

dissolution normally vanishes (see Fig. 8). Therefore, commencing dissolution would take place outside the tip region and widen the crack. Also the opposed applies: a crack that is wider than what (16) predicts, would leave upper and lower parts of the propagation front (in Fig. 8) undissolved which would give a sharper crack.

Because the stress, σ_{tip}, at the crack tip, that controls the rate of crack growth, v_{tip}, remains constant, it follows that also the crack growth rate is constant. The implication of this is that the crack growth rate remain constant even though K_{I} increase. This may seem like a paradox, but seems reasonable in view of the proportional scaling of 2ρ with $(K_{\text{I}}/\sigma_0)^2$. The effect is that the constant, and load independent, crack growth rate is a necessary requirement to maintain proportionality between volume removed material per unit of time and elastic energy release rate.

As the edge crack is growing under self-similar conditions the crack widens slowly, due to the increasing stress intensity factor. It is readily understood that this, in the extension leads to a virtually flat surface such as the initial free edge from which several cracks could be initiated. The shortest wave length of roughness growing on a surface with the stresses equal to those at the crack tip would be

$$\lambda_{\text{b}} = \frac{2\pi E\gamma}{\sigma_{\text{tip}}^2} = \frac{\lambda}{2}(\sigma_0/\sigma_{\text{tip}})^2. \tag{21}$$

Obviously branching ought to occur when at least 1.5 waves, i.e., two depressions, fit in along the blunted crack front. The stresses along the blunted tip are in the interval $4\sigma_0$ to $23\sigma_0$. Then λ_{b} is in the interval 0.06λ to 0.002λ. The reasoning that $2\rho = 1.5\lambda_{\text{b}}$ and the relation (15) between crack tip radius and the crack length, roughly predicts initiating branching when the crack length is in the interval

$$0.05\lambda < a < 1.8\lambda. \tag{22}$$

The expected crack length cannot be determined with any accuracy. The absence of branching during the present calculations to crack lengths slightly larger that 2λ is not totally unexpected considering the crude estimate made. However, branching should be expected for crack lengths of this order of magnitude.

The expected scenario after branching is that the crack continues to grow and progressively blunt until next branching occurs. The anticipated behaviour is depicted in Fig. 9. The preserved self-similar properties are interesting. They provide a picture of self-similarity such as observed for branching trees, cauliflower, coastal lines, etc.

7. Conclusions

The evolution caused by dissolution at a mechanically stressed surface is calculated. The rate of dissolution is proportional to the total available energy provided as elastic strain energy and surface energy. An adaptive finite element method is used to compute the evolution. The result agrees to some extent with earlier results, for both dissolution and surface diffusion, during incipient development of surface roughness and formation of pits. At the final stage of a pit, earlier results suggest that the body surface assumes the shape of a cycloid

with periodic array of cusps. The present result is that the cusp shape is never reached. Instead a pit continues to extend to form a crack with a finite crack tip curvature.

A single growing crack becomes self-similar, meaning that all linear dimensions of the developing crack. scale with the crack length. The width of a single crack is very small compared with the crack length. Because of the small crack width, the tip region becomes controlled by a stress intensity factor.

During the self-similar growth, the growth rate is constant even though the stress intensity factor increases. This is due to the growth rate being controlled predominantly by stresses, which remain constant during self-similar growth.

The growing cracks seem stable as long as the crack tip width is small. However, as a single crack grows and the width increases, it is predicted to branch. It is further discussed that the branching should occur repeatedly, forming a multi branched structure with self-similar properties preserved.

Acknowledgement

Support from The Knowledge Foundation under Grant No. 03/123 is acknowledged.

References

ABAQUS User's Manual, Version 6.4, Abaqus Inc., 2004.

Asaro, R.J., Tiller, W.A., 1972. Interface morphology development during stress corrosion cracking: Part I. Via surface diffusion. Metall. Trans. 3, 1789–1796, 51-978.

Materials Handbook. Corrosion, vol. 13. Academic Press.

Beech, I.B., Sunner, J., 2004. Biocorrosion: towards understanding interactions between biofilms and metals. Curr. Opinion Biotechnol. 15, 181–186.

Bjerkén, C., Ståhle, P., 2006. The path of a growing crack – a simulation of the fracture process, In: Proc. Int. Conf. Crack Paths, Parma Italy, 14–16 September, 2006.

Chiu, C.H., Gao, H.J., 1993. Stress singularities along a cycloid rough-surface. Int. J. Solids Struct. 30 (21), 2983–3012.

Grinfeld, M., 1986. Instability of the separation boundary between a non-hydrostatically stresses elastic body and a melt. Sov. Phys. Dokl. 31, 831–834.

Jivkov, A.P., 2003. A moving boundary model for fatigue corrosion cracking. In: Mammoli, A.A., Brebbia, C.A. (Eds.), Proceedings of 7th International Conference on Computational Modelling of Free and Moving Boundary Problems, November 4–6, 2003, Santa Fe, New Mexico, USA. Moving Boundaries VII, pp. 55–64.

Jivkov, A.P., 2004. The role of strain-induced passivity breakdown in corrosion crack initiation. Theor. Appl. Fract. Mech. 42 (1), 43–52.

Kim, K.-S., Hurtado, J.A., Tan, H., 1999. Evolution of a surface-roughness spectrum caused by stress in nanometer-scale chemical etching. Phys. Rev. Lett. 83 (19), 3872–3875.

Knott, G.D., 1999. Interpolating cubic splinesProgress in Computer Science and Applied Logic. Birkhauser, Boston.

Kohlert, P., Kassner, K., Misbah, C., 2002. Large amplitude behavior of Grinfeld instability. Part I: High-order weakly nonlinear analysis. Available from: <arXiv:cond-mat/0207642> v1, 26 July 2002.

MacDonald, D.D., 1999. Passivity–the key to our metal-based civilization. Pure Appl. Chem. 71 (6), 9.

Shewchuk, J.R., 2002. Delaunay refinement algorithms for triangular mesh generation. Comput. Geom. 22 (1–3), 21–74.

Spencer, B.J., Meiron, D.I., 1994. Nonlinear evolution of the stress-driven morphological instability in a 2-dimensional semiinfinite solid. Acta Metal. Mater. 42 (11), 3629–3641.

Srolovitz, D.J., 1989. On the stability of surfaces of stressed solids. Acta Metall. 37 (2), 621–625.

Yang, W.H., Srolovitz, D.J., 1994. Surface morphology evolution in stressed solids: surface diffusion controlled crack initiation. J. Mech. Phys. Solids 42 (10), 1551–1574.

Zhang, Y.W., Bower, A.F., 1999. Numerical simulations of island formation in a coherent strained epitaxial thin film system. J. Mech. Phys. Solids 47, 2273–2297.